

Fisher-information-based estimation of optomechanical coupling strengths

Claudio Sanavio,* József Zsolt Bernád, and André Xuereb
Department of Physics, University of Malta, Msida MSD 2080, Malta
 (Dated: May 28, 2024)

The formalism of quantum estimation theory, focusing on the quantum and classical Fisher information, is applied to the estimation of the coupling strength in an optomechanical system. In order to estimate the optomechanical coupling, we have considered a cavity optomechanical model with non-Markovian Brownian motion of the mirror and employed input–output formalism to obtain the cavity output field. Our estimation scenario is based on balanced homodyne photodetection of the cavity output field. We have explored the difference between the associated measurement-dependent classical Fisher information and the quantum Fisher information, thus addressing the question of whether it is possible to reach the lower bound of the mean squared error of an unbiased estimator by means of balanced homodyne detection. We have found that the phase of the local oscillator in the homodyne detection is crucial; certain quadrature measurements allow very accurate estimation.

I. INTRODUCTION

Inverse problems play an important role in science because they are able to inform us about relevant parameter values of a dynamical system that we cannot directly observe [1]. The objective of an inverse problem is to estimate these unknown parameters by extracting information from measurement data and assessing the uncertainty in these data, making use of all information known prior to the measurement process and a mathematical model of the dynamical system. In this approach, the parameters to be estimated are treated as random variables and they must be assigned a joint prior probability distribution function; this is the Bayesian formulation of the estimation problem. The qualities of estimators acting on the space of measurement data are evaluated through cost functions or, conversely, by maximizing or minimizing a cost function over the set of all possible estimators that leads to an optimal estimator. In this case, calculus of variations is applied, which is not always an easy mathematical task, especially when the estimation problem is formulated in quantum mechanics [2–4]. Applications to quantum mechanical systems do not always result in an experimentally implementable optimal estimator [5–9].

Optimal estimators, in general, are likely to be complicated, as is observed in our previous investigation on the estimation of the nonlinear optomechanical coupling strength [7]. Furthermore, solving the variational problem for the average cost function imposes limits on the use of models with many types of decoherence sources. In order to work with more effective models of cavity optomechanical systems [10] and to consider experimentally relevant estimation strategies [11], one has to turn to the investigation of the lower bounds of some convenient measure of the estimation accuracy. The mean-squared error- the average squared difference between estimated values and true values of the unknown parameters- is

usually employed as a measure of accuracy. In the case of classical systems, there are some complicated lower bounds of the mean-squared error [12, 13]; however, the Cramér–Rao inequality [14, 15], which defines an inferior but a simpler lower bound, can be extended to quantum systems [16]. Here, the lower bound is inversely proportional to the quantum Fisher information (QFI), irrespective of whether the estimator is biased or unbiased; see Ref. [9]. The chosen estimation strategy, expressed as a positive-operator valued measure (POVM), provides probability distributions of the parameter to be estimated, conditioned on the true value of this parameter. These probabilities determine the classical Fisher information (CFI), which is inversely proportional to the lower bound of the mean-squared error in the classical post-processing of measurement data. As the CFI is always smaller than or equal to the QFI, which defines the smallest value of the lower bound, it is worthwhile to investigate the circumstances where the CFI is as close as possible to the QFI [17]. If the QFI is saturated by some POVM and the probability distributions belong to a one-parameter exponential family, which is a requirement that our theoretical approach fulfills, then there exists a suitable classical unbiased estimator on the measurement data [18], which saturates the CFI and thus yields the most precise measurement.

In this paper, we follow the above-described methodology, which allows us to consider a detailed model of a cavity optomechanical system. We consider a single mode of the radiation field inside a cavity and also a single vibrational mode of the mechanical resonator. The two modes interact via a radiation-pressure interaction Hamiltonian [19]. The single-mode field assumption is justified when the cavity is driven by an external laser with a bandwidth significantly narrower than the separation among the different electromagnetic field modes. The laser populates only one mode, allowing us to neglect the others. There are many mechanical modes, but describing only one of them has proven to be a valid approximation in experiment [10]. The mechanical oscillator is subject to quantum Brownian motion [20, 21] and the single-mode cavity field is coupled to the electromag-

*Electronic address: claudio.sanavio@um.edu.mt

netic field outside of the cavity [22]. Finally, balanced homodyne photodetection with non-ideal detectors [23] is carried out on the output field; this automatically defines the set of POVMs, i.e., the estimation strategy, that we explore. We investigate the QFI of the output field state depending on the unknown value of the nonlinear optomechanical coupling and compare with the CFI obtained from the data provided by the balanced homodyne photodetection. We identify those cases where CFI is as large as possible, where the lower bound of the estimation accuracy is therefore smallest.

This paper is organized as follows. In Sec. II, we discuss the cavity optomechanical model and determine the stationary state of the output field. In Sec. III, the QFI of the output field state is determined. A brief overview of balanced homodyne photodetection and the related POVM is presented and probabilities of these measurements are given, which allows us to calculate the CFI. A numerical investigation and the maximization of CFI with respect to QFI are addressed in Sec. IV. Finally, in Sec. V, we draw conclusions and make some remarks on our work. Detailed derivations supporting the main text are collected in the two appendices.

II. MODEL

The optomechanical system we have in mind is formed by a Fabry–Pérot cavity with a moving-end mirror and we focus on a case where only a single mode of the radiation field and a vibrational mode of the mechanical oscillator, i.e., moving mirror, are considered. The model can be used to describe several alternative systems [10]. The free Hamiltonian of the system reads

$$\hat{H}_0 = \hbar\omega_c \hat{a}^\dagger \hat{a} + \frac{\hat{p}^2}{2m} + \frac{1}{2}m\omega_m^2 \hat{q}^2, \quad (1)$$

where \hat{q} and \hat{p} are position and momentum operators for the mechanical oscillator of effective mass m and which oscillates at frequency ω_m . The annihilation and creation operators of the single-mode radiation field with frequency ω_c are denoted by \hat{a} and \hat{a}^\dagger . The two subsystems are coupled by the optomechanical interaction [19], which is the radiation pressure on the oscillating mirror, which is well described by a non-linear Hamiltonian term [10],

$$\hat{H}_I = -\hbar g \hat{a}^\dagger \hat{a} \hat{q}, \quad (2)$$

with coupling strength g . The use of the term “non-linear” here refers to the equation of motion of the system operators, at least one of which is non-linear, and is related to the Hamiltonian being of third order in these operators.

In order to describe this optomechanical system effectively, one has to consider decoherence and excitation losses, i.e., the concept of open quantum systems has to be applied. The single-mode field is affected by a decay

with rate $\kappa = \kappa_{\text{in}} + \kappa_{\text{loss}}$, where κ_{in} is the loss rate associated with the input–output fields and κ_{loss} is related to what are commonly called internal losses [24]. The latter quantity could, for example, originate from the fact that the cavity mirrors act to scatter photons from the cavity mode of interest to other modes or to the outside environment. The mechanical oscillator is in contact with a phonon bath at temperature T and experiences a friction or decay rate γ . The dynamics is given in the Heisenberg picture with the use of the quantum Langevin equations,

$$\dot{\hat{a}} = -i\omega_c \hat{a} + ig\hat{a}\hat{q} - \frac{\kappa}{2}\hat{a} + \sqrt{\kappa_{\text{in}}}\hat{a}_{\text{in}} + \sqrt{\kappa_{\text{loss}}}\hat{a}_{\text{loss}}, \quad (3)$$

$$\dot{\hat{a}}^\dagger = i\omega_c \hat{a}^\dagger - ig\hat{a}^\dagger \hat{q} - \frac{\kappa}{2}\hat{a}^\dagger + \sqrt{\kappa_{\text{in}}}\hat{a}_{\text{in}}^\dagger + \sqrt{\kappa_{\text{loss}}}\hat{a}_{\text{loss}}^\dagger, \quad (4)$$

$$\dot{\hat{q}} = \frac{\hat{p}}{m}, \quad (5)$$

$$\dot{\hat{p}} = -m\omega_m^2 \hat{q} - \gamma\hat{p} + \hbar g \hat{a}^\dagger \hat{a} + \hat{\xi}. \quad (6)$$

where \hat{a}_{in} is the input noise operator associated with the modes of the radiation field outside the cavity. \hat{a}_{loss} is the operator describing the internal losses and $\hat{\xi}$ represents the quantum Brownian noise operator. Making use of the spectral density $J(\omega)$ of the phonon modes in the bath and the weak coupling of the mechanical oscillator to the bath [25], one can define the following functions [26]:

$$\mathfrak{D}_R(\tau) = \int_0^\infty d\omega J(\omega) \cos(\omega\tau) \coth\left(\frac{\hbar\omega}{2k_B T}\right) \quad (7)$$

$$\mathfrak{D}_I(\tau) = \int_0^\infty d\omega J(\omega) \sin(\omega\tau). \quad (8)$$

Now, we are able to calculate the two-time correlation function of $\hat{\xi}(t)$,

$$\langle \hat{\xi}(t)\hat{\xi}(t') \rangle = \hbar[\mathfrak{D}_R(t-t') - i\mathfrak{D}_I(t-t')]. \quad (9)$$

The mean of $\hat{\xi}(t)$ is zero and its non-Markovian nature allows us to preserve the correct commutation relations between \hat{p} and \hat{q} during the time evolution [26]. An extensively studied case is the ohmic spectral density with a Lorentz–Drude cutoff function,

$$J(\omega) = \frac{2m\gamma}{\pi} \omega \frac{\Omega^2}{\omega^2 + \Omega^2},$$

where Ω is the high-frequency cutoff. An ohmic spectral density with exponential cutoff [27],

$$J(\omega) = \frac{2m\gamma}{\pi} \omega \exp\left(-\frac{\omega}{\Omega}\right) \quad (10)$$

leads to very similar behavior to one with a Lorentz–Drude cutoff function, albeit with the advantage that the integrations in Eqs. (7) and (8) have analytical solutions

in closed form,

$$\begin{aligned}\mathfrak{D}_R(\tau) &= \frac{2m\gamma}{\pi} \frac{\Omega^2 (\Omega^2 \tau^2 - 1)}{(\Omega^2 \tau^2 + 1)^2} + \\ &\quad \frac{2m\gamma}{\pi \hbar^2} (k_B T)^2 \left[\Psi^{(1)}(z) + \Psi^{(1)}(z^*) \right], \\ z &= \frac{1 - i\Omega\tau}{\hbar\Omega} k_B T, \\ \mathfrak{D}_I(\tau) &= \frac{2m\gamma}{\pi} \frac{2\Omega^3 \tau}{(\Omega^2 \tau^2 + 1)^2}\end{aligned}$$

with $\Psi^{(1)}(z)$ being the polygamma function [28]. The cavity operates at optical frequencies, i.e., $\hbar\omega_c/k_B T \gg 1$ holds to a very good approximation at reasonable temperatures, and therefore the operators $\hat{a}_{\text{in}}(t)$ and $\hat{a}_{\text{in}}^\dagger(t')$ commute for $t \neq t'$. Their correlation functions in the vacuum state $|0\rangle$ read

$$\begin{aligned}\langle 0 | \hat{a}_{\text{in}}(t) \hat{a}_{\text{in}}^\dagger(t') | 0 \rangle &= \delta(t - t'), \\ \langle 0 | \hat{a}_{\text{in}}^\dagger(t') \hat{a}_{\text{in}}(t) | 0 \rangle &= 0.\end{aligned}$$

The operators $\hat{a}_{\text{loss}}(t)$ and $\hat{a}_{\text{loss}}^\dagger$ have similar commutation relations and, furthermore, they commute at all times with $\hat{a}_{\text{in}}(t)$ and $\hat{a}_{\text{in}}^\dagger(t')$.

Usually the single mode of the cavity is driven by a laser with frequency ω_L and intensity ϵ . This process can be modified through the addition of the following term to the Hamiltonian:

$$H_L = i\hbar\epsilon (\hat{a}^\dagger e^{-i\omega_L t} - \hat{a} e^{i\omega_L t}), \quad (11)$$

whose phases $\pm\omega_L t$ can be easily absorbed after going into a rotating frame, with a resulting detuning for the optical frequency $\Delta_0 = \omega_c - \omega_L$. In terms of the power P of the laser, the driving intensity is $\epsilon = \sqrt{2\kappa_{\text{in}} P / \hbar\omega_L}$.

It is worth noting that the driving of the field is a necessary condition to obtain an effectively linear optomechanical interaction [10]. The application of a high-intensity laser field causes the single-mode field to reach a steady state with finite amplitude α ($|\alpha| \gg 1$) and allows us to consider only the quantum fluctuations around this stationary state. This also affects the mechanical oscillator by shifting the minimum of the harmonic potential. The dynamics of the fluctuations around the steady state is well described by linearizing the quantum Langevin equations (3)–(6). This can mathematically be described by the application of two displacement operators ,

$$\hat{D}_1(\alpha) = e^{\alpha \hat{a}^\dagger - \alpha^* \hat{a}} \quad \text{and} \quad \hat{D}_2(\beta_0) = e^{\beta_0 \hat{b}^\dagger - \beta_0^* \hat{b}}$$

with

$$\hat{b} = \sqrt{\frac{m\omega_m}{2\hbar}} \left(\hat{q} + \frac{i}{m\omega_m} \hat{p} \right) \quad (12)$$

$$\hat{b}^\dagger = \sqrt{\frac{m\omega_m}{2\hbar}} \left(\hat{q} - \frac{i}{m\omega_m} \hat{p} \right) \quad (13)$$

on the quantum Langevin equations (3)–(6). The above equations also define relations between (β_0, β_0^*) and

(q_0, p_0) . A transformation back to the operators \hat{p} and \hat{q} , with the quantities introduced above satisfying the non-linear equation

$$i\epsilon = -\Delta_0 \alpha + g\alpha q_0 - i\frac{\kappa}{2} \alpha \quad (14)$$

yields a driving free Hamiltonian,

$$\hbar\Delta \hat{a}^\dagger \hat{a} + \frac{\hat{p}^2}{2m} + \frac{1}{2} m\omega_m^2 \hat{q}^2 - \hbar g\alpha (\hat{a} + \hat{a}^\dagger) \hat{q}, \quad (15)$$

where

$$\Delta = \Delta_0 - \hbar \frac{g^2 |\alpha|^2}{m\omega_m^2}, \quad (16)$$

$$q_0 = \hbar \frac{g |\alpha|^2}{m\omega_m^2}. \quad (17)$$

Equation (14), together with the above equations, yields a third degree equation for $|\alpha|$. Depending on the value of the power P , we may encounter a bistability of the system that will give two different solutions for the shift in the rest position of the mirror (17). One should note that the steady-state amplitude depends on the value of g , making α a function of g , i.e. $\alpha = \alpha(g)$. The same is valid for the detuning $\Delta = \Delta(g)$. Therefore, for a fixed value of P , the bistability also depends explicitly on g , which is as yet unknown. A good strategy here is to define an interval, depending on our prior knowledge, for the possible values of g and adjust the power of laser P such that the bistability is completely avoided. For detailed calculations and regions of stability and bistability, see Appendix A.

The shifted operators (also denoted fluctuation operators) $\delta\hat{a} = \hat{a} - \alpha$ and $\delta\hat{q} = \hat{q} - q_0$ are subject to the same loss process as the original ones. Note that the momentum operator $\delta\hat{p} = \hat{p}$ is not changed because β_0 is real, which implies that $p_0 = 0$. It is more convenient to define the two quadratures of the single-mode field $\delta\hat{X} = (\delta\hat{a}^\dagger + \delta\hat{a})/\sqrt{2}$ and $\delta\hat{Y} = i(\delta\hat{a}^\dagger - \delta\hat{a})/\sqrt{2}$. We analogously define the quadratures \hat{X}_{in} , \hat{Y}_{in} , \hat{X}_{loss} , and \hat{Y}_{loss} . Under the assumption that $|\alpha|$ is large, we can truncate the equations of motion to first order in the fluctuation operators. Finally, the differential equations of the shifted operators can be written in the concise form

$$\dot{u}(t) = Au(t) + \eta(t), \quad (18)$$

where we have defined the vector of operators $u(t) = (\delta\hat{q}(t), \delta\hat{p}(t), \delta\hat{X}(t), \delta\hat{Y}(t))^T$ and

$$\begin{aligned}\eta(t) &= \left(0, \hat{\xi}(t), \sqrt{\kappa_{\text{in}}} \hat{X}_{\text{in}}(t) + \sqrt{\kappa_{\text{loss}}} \hat{X}_{\text{loss}}(t), \right. \\ &\quad \left. \sqrt{\kappa_{\text{in}}} \hat{Y}_{\text{in}}(t) + \sqrt{\kappa_{\text{loss}}} \hat{Y}_{\text{loss}}(t) \right)^T;\end{aligned}$$

and the superscript T denotes the transposition. Furthermore, we have

$$A = \begin{pmatrix} 0 & \frac{1}{m} & 0 & 0 \\ -m\omega_m^2 & -\gamma & \sqrt{2}\hbar g\alpha(g) & 0 \\ 0 & 0 & -\frac{\kappa}{2} & \Delta(g) \\ \sqrt{2}g\alpha(g) & 0 & -\Delta(g) & -\frac{\kappa}{2} \end{pmatrix} \quad (19)$$

where we have introduced the explicit dependence of $\alpha(g)$ and $\Delta(g)$ on g . The solution to (18) reads

$$u(t) = \exp(At)u(0) + \int_0^t dt' \exp[A(t-t')] \eta(t'). \quad (20)$$

The autocorrelation matrix is given by

$$R(t, s) = \langle u(t)u(s)^T \rangle.$$

Making use of the relation

$$\langle u(0)\eta(t)^T \rangle = \langle \eta(t)u(0)^T \rangle = 0, \quad t \geq 0,$$

one finds

$$R(t, s) = \exp(At) \langle u(0)u(0)^T \rangle \exp(A^T s) + \int_0^t \int_0^s dt' dt'' \exp[A(t-t')] M(t' - t'') \exp[A^T(s-t'')]$$

where

$$M(t' - t'') = \langle \eta(t')\eta(t'')^T \rangle = \begin{pmatrix} 0 & 0 & 0 & 0 \\ 0 & \langle \hat{\xi}(t')\hat{\xi}(t'') \rangle & 0 & 0 \\ 0 & 0 & \frac{\kappa}{2}\delta(t' - t'') & i\frac{\kappa}{2}\delta(t' - t'') \\ 0 & 0 & -i\frac{\kappa}{2}\delta(t' - t'') & \frac{\kappa}{2}\delta(t' - t'') \end{pmatrix}.$$

Let us consider the symmetric autocorrelation matrix

$$\sigma(t, s) = \frac{R(t, s) + R^T(t, s)}{2}.$$

Taking $t = s$ we obtain

$$\frac{d}{dt}\sigma(t) = A\sigma(t) + \sigma(t)A^T + D(t),$$

where $\sigma(t) \equiv \sigma(t, t)$, and with

$$D(t) = \int_0^t dt' \frac{M(t-t') + M^T(t-t')}{2} \exp[A^T(t-t')] + \int_0^t dt' \exp[A(t-t')] \frac{M(t'-t) + M^T(t'-t)}{2}.$$

This can be further simplified via

$$M_1(t-t') = \frac{M(t-t') + M^T(t-t')}{2} = \begin{pmatrix} 0 & 0 & 0 & 0 \\ 0 & \hbar \mathfrak{D}_R(t-t') & 0 & 0 \\ 0 & 0 & \frac{\kappa}{2}\delta(t-t') & 0 \\ 0 & 0 & 0 & \frac{\kappa}{2}\delta(t-t') \end{pmatrix},$$

because $\mathfrak{D}_R(-t) = \mathfrak{D}_R(t)$ and $\mathfrak{D}_I(-t) = -\mathfrak{D}_I(t)$, which also implies

$$M_1(t-t') = M_1(t'-t).$$

Finally, we can write

$$D(t) = \int_0^t d\tau [M_1(\tau) \exp(A^T \tau) + \exp(A\tau) M_1(\tau)].$$

The stability of the system, $\lim_{t \rightarrow \infty} \exp(At) = 0$, can be derived by applying the Routh–Hurwitz criterion [29]. This has been thoroughly investigated in the last decade and the two nontrivial conditions on the parameters of A show that if the system is stable, then the bistability of the dynamics is avoided [30]. From now on, we consider these conditions to be satisfied. Therefore, $u(t)$ for $t \rightarrow \infty$ approaches zero, which implies that the autocorrelation matrix $\sigma(t)$ coincides with the matrix in the stationary solution. The stationary correlation matrix is defined as $\sigma = \lim_{t \rightarrow \infty} \sigma(t, t)$ and is the solution to the following Lyapunov equation:

$$A\sigma + \sigma A^T = -D, \quad (21)$$

where

$$D = \int_0^\infty d\tau [M_1(\tau) \exp(A^T \tau) + \exp(A\tau) M_1(\tau)].$$

We need to keep in mind that any experimental apparatus does not have direct access to the cavity field, but only to the output field, which escapes the cavity. We can calculate the fluctuations of this field around its stationary state with the use of the input–output relations,

$$\hat{a}_{\text{out}} = \sqrt{\kappa_{\text{in}}} \delta \hat{a} - \hat{a}_{\text{in}}. \quad (22)$$

In practice, one selects different modes by opening a filter in a certain interval of time or in different frequency intervals. Hence, we can define N -independent output modes following the approach of Ref. [30],

$$\hat{a}_{k,\text{out}}(t) = \int_{-\infty}^t ds g_k(t-s) \hat{a}_{\text{out}}(s), \quad k = 1, \dots, N, \quad (23)$$

where $g_k(s)$ is the filter function defining the k^{th} mode. Here we will make use of the filter function,

$$g_k(t) = \frac{\theta(t) - \theta(t-\tau)}{\sqrt{\tau}} e^{-i\Omega_k t}, \quad (24)$$

with $\Omega_j - \Omega_l = \frac{2\pi}{\tau} n$, $n \in \mathbb{N}$. The k^{th} mode is centered at the frequency Ω_k and has a bandwidth $1/\tau$. Making use of the input–output relations (22), we obtain the correlation matrix $\sigma_{k,\text{out}}$ of the output field quadratures $\hat{X}_{k,\text{out}}$ and $\hat{Y}_{k,\text{out}}$ related to a filter centered at frequency Ω_k as (see Appendix B)

$$\langle \hat{X}_{k,\text{out}} \hat{X}_{k,\text{out}} \rangle(\tau) = \frac{1}{2} \kappa \tau \text{sinc}^2 \left(\frac{\Omega_k \tau}{2} \right) [(\sigma_{xx} - \sigma_{yy}) \cos(\Omega_k \tau) + \sigma_{xx} + 2\sigma_{xy} \sin(\Omega_k \tau) + \sigma_{yy}] + \text{sinc}(2\Omega_k \tau) \quad (25)$$

$$\langle \hat{X}_{k,\text{out}} \hat{Y}_{k,\text{out}} \rangle(\tau) = \frac{1}{2} \kappa \tau \text{sinc} \left(\frac{\Omega_k \tau}{2} \right)^2 [(\sigma_{yy} - \sigma_{xx}) \sin(\Omega_k \tau) + 2\sigma_{xy} \cos(\Omega_k \tau)] \quad (26)$$

$$\langle \hat{Y}_{k,\text{out}} \hat{Y}_{k,\text{out}} \rangle(\tau) = \frac{1}{2} \kappa \tau \text{sinc}^2 \left(\frac{\Omega_k \tau}{2} \right) [(\sigma_{yy} - \sigma_{xx}) \cos(\Omega_k \tau) + \sigma_{xx} - 2\sigma_{xy} \sin(\Omega_k \tau) + \sigma_{yy}] + \text{sinc}(2\Omega_k \tau) \quad (27)$$

where $\sigma_{AB} = \langle \delta \hat{A} \delta \hat{B} \rangle$ ($A, B \in \{X, Y\}$) are the entries of matrix σ , which are obtained in Eq. (21), and $\text{sinc}(x)$ is the unnormalized sinc function $\text{sinc}(x) = \sin(x)/x$. The shifted operators are fully characterized in the stationary state by the correlation matrix, since all noises involved obey this property and the equations of motion are linear. One can thus deduce that their properties can also be described by a zero-mean Gaussian state. Similarly, the output field fluctuations are given by the Gaussian Wigner function

$$W(\xi) = \frac{1}{\sqrt{2\pi \det(\sigma_{k,\text{out}})}} e^{-\frac{1}{2} \xi^T \sigma_{k,\text{out}}^{-1} \xi}, \quad (28)$$

where $\xi = (X_{k,\text{out}}, Y_{k,\text{out}})^T$ and $\sigma_{k,\text{out}}$ is the correlation matrix. The above Wigner function depends on the optomechanical coupling strength g through $\sigma_{k,\text{out}}$, and is a function of the correlation matrix of the cavity optomechanical system. In our subsequent discussion, we analyze Eq. (28) in the context of a quantum estimation strategy based on the quantum Fisher information. Our task will be to seek optimal balanced homodyne photodetection measurement strategies.

III. QUANTUM AND CLASSICAL FISHER INFORMATION

In this section, we derive the quantum Fisher information (QFI) H_g of the optomechanical coupling strength for a general Gaussian state, employing the phase-space description provided by the Wigner quasiprobability distribution (28). The QFI defines a lower bound for the mean-squared error (MSE) of an estimation setup, which is ensured by the quantum Cramér–Rao theorem [16],

$$\text{MSE}(g) \geq \frac{|x'(g)|^2}{H_g}, \quad (29)$$

where $x'(g)$ is the derivative of the average estimator. When the estimator is unbiased, then $x'(g) = 1$. The QFI is given as

$$H_g = \text{Tr}[\hat{\rho} \hat{L}_g^2], \quad (30)$$

where \hat{L}_g is the symmetric logarithmic derivative (SLD) defined by the equation

$$\partial_g \hat{\rho} = \frac{1}{2} \{\hat{\rho}, \hat{L}_g\}. \quad (31)$$

We are going to use this general formalism to the Gaussian state obtained in Eq. (28). A Gaussian state is completely determined by its first and second moments; however, here we have that the first moment is zero, following the argument in Sec. II. Since the density operator $\hat{\rho}$ of a Gaussian state can be expressed in an exponential form [31], we can write the operator \hat{L}_g as a function of the covariance matrix $\sigma_{k,\text{out}}$. We neglect all subscripts in the subsequent discussion because, from now on, we focus on one mode of the electromagnetic field that is detected.

In order to find the SLD, we use the Weyl transform on the operator, obtaining

$$L(x, p) = \xi^T \Phi \xi - \nu, \quad (32)$$

where the explicit forms of Φ and ν are

$$\Phi = -\frac{1}{2} \partial_g (\sigma^{-1}) \quad (33)$$

$$\nu = -\frac{1}{2} \partial_g \ln(\det \sigma) = \text{Tr}[\Phi \sigma]. \quad (34)$$

It is worth noticing that the quadratic nature of $L(x, p)$ is ensured by the Gaussian form of $W(x, p)$.

We use the SLD to calculate the QFI H_g related to the parameter g following Eq. (30). However, the calculation of the Weyl transform of \hat{L}_g^2 is not straightforward. In order to calculate it, we need to Weyl transform the function $L(x, p)$ back to the operator \hat{L}_g , yielding

$$\hat{L} = \Phi_{11} \hat{x}^2 + \Phi_{12} (\hat{x} \hat{p} + \hat{p} \hat{x}) + \Phi_{22} \hat{p}^2 - \nu \mathbb{1}. \quad (35)$$

Now, one is able to calculate \hat{L}_g^2 and after performing the symmetric ordering and the Weyl transform on it, we find $L^{(2)}(x, p)$ as

$$\begin{aligned} L^2(x, p) = & \Phi_{11}^2 x^4 + 4\Phi_{11}\Phi_{12} p x^3 + 4\Phi_{12}^2 p^2 x^2 \\ & + 2\Phi_{11}\Phi_{22} p^2 x^2 + 4\Phi_{12}\Phi_{22} p^3 x + \Phi_{22}^2 p^4 \\ & - 2\nu L(x, p) - \nu^2 - \frac{1}{2} \det(\Phi). \end{aligned} \quad (36)$$

The QFI obtained as the mean value of \hat{L}^2 on the state $\hat{\rho}$ can be calculated by the phase-space formalism,

$$\begin{aligned} H(g) = & \int dx dp L^{(2)}(x, p) W(x, p) \\ = & 3\text{Tr}[(\Phi \sigma)^2] - 2\nu \text{Tr}[\Phi \sigma] + 2 \det(\sigma) \det(\Phi) \\ & - \frac{1}{2} \det(\Phi) + \nu^2. \end{aligned} \quad (37)$$

We will make use of Eq. (37) to determine the QFI of the output field. Combining together (37) and (33), we obtain the QFI for a two-dimensional Gaussian state with zero mean,

$$H(g) = \frac{1}{2} \text{Tr}[(\partial_g(\sigma^{-1})\sigma)^2] - \frac{1}{8} \det[\partial_g(\sigma^{-1})]. \quad (38)$$

The quantum Cramér–Rao bound (29) for an unbiased estimator is saturated only if we implement the best strategy (POVM) that minimizes the MSE of the parameter estimation. This strategy is usually very difficult to find and may be impossible to implement [7]. However, we can find, for each practical measurement strategy, the maximum amount of Fisher information it can provide. Measurements on quantum systems provide a probability density function which depends on the parameter to be estimated. The amount of information on the unknown parameter carried by this probability density function can be measured by the so-called classical Fisher information (CFI)

$$F_g = \int dx P(x; g) \left(\partial_g \ln P(x; g) \right)^2, \quad (39)$$

where $P(x; g)$ is the probability of obtaining the output of the measure x when the true value of the parameter is g . In quantum mechanics, this probability is given by the relation $P(x; g) = \text{Tr}[\hat{\rho}_g \Pi_x]$. Here, we consider that the measurements are performed by balanced homodyne photodetection (BHD) [23]. This makes use of two photodetectors, each with quantum efficiency η . In BHD, the data recorded are proportional to the difference of the measured photon numbers $n_{1,2}$ of the two photodetectors, yielding

$$P_\theta(n; g) = \sum_{m=0}^{\infty} \langle : e^{-\eta(\hat{n}_1 + \hat{n}_2)} \frac{(\eta \hat{n}_1)^{n+m}}{(n+m)!} \frac{(\eta \hat{n}_2)^m}{m!} : \rangle_{\hat{\rho}_g \otimes \hat{\rho}_{LO}}$$

where $\hat{\rho}_{LO}$ is the state of the local oscillator, considered to be a coherent state $\hat{\rho}_{LO} = |\alpha_{LO}\rangle\langle\alpha_{LO}|$. The symmetric order denoted by $::$ helps us to find the Weyl transform of the element $\Pi_k^\eta(x, p)$ of the BHD POVM,

$$\Pi_k^\eta(x, p) = \exp \left[-\frac{2\eta \left(k - \frac{x \cos \theta + p \sin \theta}{\sqrt{2}} \right)^2}{1 - \eta} \right] \quad (40)$$

obtained in the limit of $|\alpha_{LO}| \gg 1$. The parameter θ is the angle of the coherent state $|\alpha_{LO}\rangle$, i.e., $\theta = \arg(\alpha_{LO})$, and defines the quadrature that is measured. The probability is

$$P_\theta^\eta(k; g) = \sqrt{\frac{2\eta}{\pi(1-\eta)}} \int dx dp W(x, p) \Pi_k^\eta(x, p). \quad (41)$$

Using the condition (28) for the Wigner function leads to

$$P_\theta^\eta(k; g) = \frac{1}{\pi} \sqrt{\frac{2\eta}{1-\eta+2\eta R_\theta^T \sigma R_\theta}} e^{-\frac{2\eta k^2}{1-\eta+2\eta R_\theta^T \sigma R_\theta}},$$

where we have defined $R_\theta = (\cos \theta, \sin \theta)^T$. Now, we can calculate the CFI with the help of Eq. (39), yielding

$$F_g^\eta = 2 \left(\frac{\eta R_\theta^T \partial_g \sigma R_\theta}{1 - \eta + 2\eta R_\theta^T \sigma R_\theta} \right)^2. \quad (42)$$

Equation Eq. (42) is a compact form for the classical Fisher information of the BHD. Notice that in the case of perfect detectors ($\eta \rightarrow 1$) Eq. (40) reduces to a Dirac delta $\Pi_k^1(x, p) \rightarrow \delta(k - R^T \xi)$. In this case, the CFI assumes the form

$$F_g^1 = \left(\frac{R_\theta^T \partial_g \sigma R_\theta}{R_\theta^T \sigma R_\theta} \right)^2. \quad (43)$$

IV. RESULTS

In Sec. II, we have calculated the covariance matrix (25) of the output field escaping the cavity and characterized by the filter function (24). In Sec. III, we have calculated the general form of the quantum Fisher information (QFI) of Gaussian states with zero mean, like the output field, and the classical Fisher information (CFI) of balanced homodyne photodetection (BHD) measurements. In this section, we numerically investigate and compare QFI and CFI for an experimentally feasible situation. We consider the cavity to possess equal internal and external decay rates, $\kappa_{\text{in}} = \kappa_{\text{loss}} = \kappa$, and our detector to stay on for a temporal window of length $\tau = 1/\kappa$. For our numerical analysis, we take the experimental values from [32], which are $\kappa/2\pi = 18.5$ MHz, $\gamma/2\pi = 130$ Hz, $\omega_m/2\pi = 1.14$ MHz, $T = 11$ K, $m = 16$ ng, and the power of the laser, $P = 1$ μ W. Although the subject is to estimate the optomechanical coupling strength, we still need to set a central value around which we conduct our investigations. The coupling strength g in Eq. (2) has the dimensions of $[\text{Hz} \cdot \text{m}^{-1}]$, whereas in the experimental community, it is common to give the dimensions of g in Hertz [10]. We solve this by carrying out the transformation $g \rightarrow g \sqrt{\frac{2m\omega_m}{\hbar}}$. Now, this transformed value according to Ref. [32] is $g/2\pi = 129$ Hz. In order to work in the high-temperature limit $k_B T \gg \hbar \Omega \gg \hbar \omega_m$, we set the cutoff frequency Ω in Eq. (10) to $5\omega_m$. In our subsequent numerical investigations, the detuning Δ_0 is always chosen in such a way that bistability of the mechanical oscillator is avoided [33]. As a next step, we need to understand which central frequency of the filter function Ω_k gives us the best accuracy on the estimation of the coupling strength g . Therefore, we have calculated QFI as a function of Ω_k , which has a peak at $\Omega_k = 0$, as shown in Fig. 1. Since we are in the rotating frame, this means that our detector filter function peaks at the laser frequency ω_L .

Our goal is to find conditions for which the BHD results in the best achievable estimation strategy. This would correspond to the saturation of the quantum Cramér–Rao bound. The outcome of the BHD depends on the

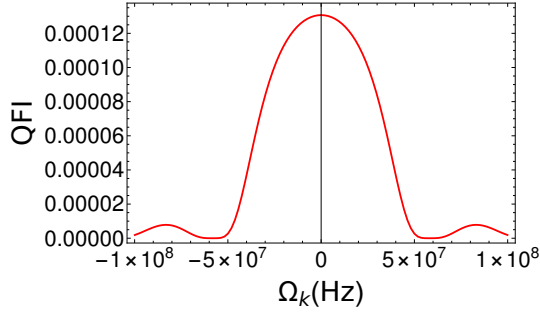


FIG. 1: Quantum Fisher information (QFI) as a function of the filter function's center frequency Ω_k . In the rotating frame the peak of QFI is at $\Omega_k = 0$, which corresponds to maximum accuracy reached in the estimation scenario. This also means that in the laboratory frame measurements should be performed around the frequency of the driving laser ω_L . The parameters are $\kappa/2\pi = 18.5$ MHz, $\gamma/2\pi = 130$ Hz, $g/2\pi = 129$ Hz, $\omega_m/2\pi = 1.14$ MHz, $m = 16$ ng, $T = 11$ K, $\Delta_0 = -2\kappa$ and the cutoff frequency $\Omega = 5\omega_m$.

quantum efficiency of the detectors η and on the quadrature phase θ that we choose to measure. Figure 2 shows the CFI as a function of these parameters. We notice that in the case of ideal detectors, i.e., $\eta = 1$, the optimal choice for the phase $\theta = \theta_{\max}$ leads the CFI to saturate the upper limit given by the QFI. This is a remarkable result that allows us to consider BHD as the optimal measurement that gives us the best estimate of g . In fact, Fig. 2(b) shows that the detector's efficiency η is a very important parameter that affects the quality of the measurement, although it is no surprise that ideal photodetection results in an optimal measurement scenario.

In general, an analytical solution for θ_{\max} is very cumbersome because the global maximum of either Eq. (42) or Eq. (43) depends on the entries of σ in Eq. (28), which are very complicated functions of the parameters of the system. However, the angle θ_{\max} can be understood in the following way. Let us consider (43), which is the square of a generalized Rayleigh quotient for the self-adjoint matrix pairs $(\partial_g \sigma, \sigma)$ (see, for example, Ref. [34]). Assuming that σ is positive definite, i.e., does not describe a pure state, we would like to maximize

$$f(\theta) = \frac{R_\theta^T \partial_g \sigma R_\theta}{R_\theta^T \sigma R_\theta}. \quad (44)$$

The maximum value that $f(\theta)$ can reach is the maximum eigenvalue λ_{\max} of $\sigma^{-1/2} \partial_g \sigma \sigma^{-1/2}$ when R_θ is equal to the corresponding eigenvector v_{\max} , which automatically defines θ_{\max} . In the case of (42), we have a squared sum of generalized Rayleigh quotients [35], and now, θ_{\max} can mostly be found by computational efforts.

Our numerical investigations show that the value of θ_{\max} is most sensitive to changes in the value of detuning Δ_0 as well of the central frequency of the filter function Ω_k . In order to gain some insight, we show in Fig. 3(a) the dependence of θ_{\max} with respect to Ω_k . We can see

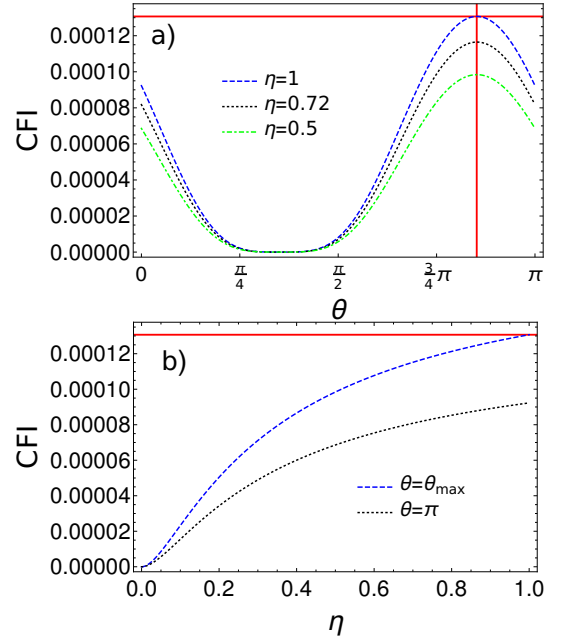


FIG. 2: a) Classical Fisher information (CFI) as a function of the local oscillator phase θ in the homodyne measurement for different values of η . b) CFI as a function of η for two different choices of θ . $\Omega_k = 0$ and the rest of the parameters are the same of Fig. 1.

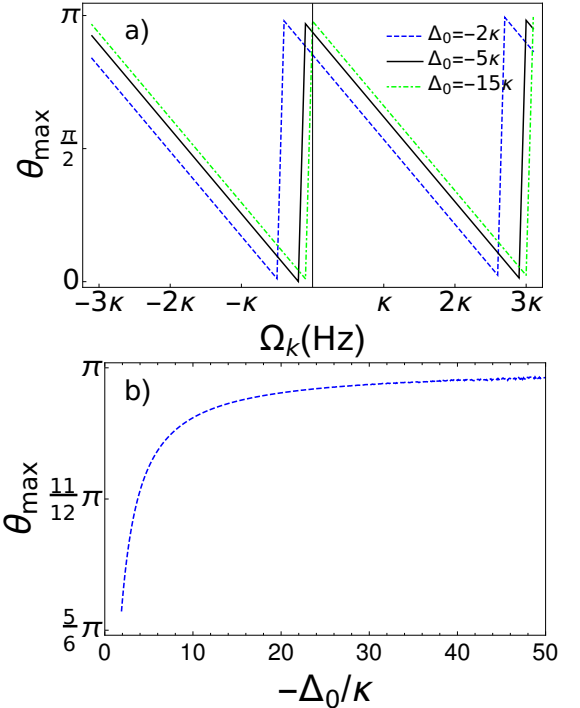


FIG. 3: (a) The quadrature phase θ_{\max} as a function of the filter function's center frequency Ω_k and for different values of the detuning Δ_0 . (b) θ_{\max} as a function of the detuning Δ_0 for $\Omega_k = 0$. All other parameters are the same of Fig. 1.

that θ_{\max} as a function of Ω_k follows an inverted ramp function. The ramp starts at κ^2/Δ_0 and has a period of 3κ . In the limit $\Delta_0 \rightarrow -\infty$, θ_{\max} tends to π . This is demonstrated in Fig. 3(b), which shows the value of θ_{\max} as a function of the ratio $-\Delta_0/\kappa$.

In the case of ideal detectors, i.e. $\eta = 1$, and choosing $\theta = \theta_{\max}$, the curve of CFI as a function of Ω_k perfectly overlaps with the curve of QFI in Fig. 1. Thus, we can definitely set $\Omega_k = 0$ for the rest of our numerical analysis because this choice guarantees the maximum accuracy in the estimation scenario. Now, we show the CFI, calculated numerically as we vary selected parameters that appear in the dynamical matrix A of Eq. (19). The ranges of the plots are given by the stability conditions imposed on the system. Figures 4(a) and 4(b) show the CFI as a function of the optical and mechanical decay rate, respectively. These curves illustrate that increasing the decay rates lowers the accuracy of the estimation of the optomechanical coupling strength g . The opposite behavior is obtained increasing the power of the driving laser P ; see Fig. 4(c). In this case, a higher P leads to a higher value for the stationary field amplitude $|\alpha|$, which leads to a more significant contribution to the dynamics from the optomechanical interaction as it appears in the interaction Hamiltonian (2). Figure 4(d) shows the CFI for different values of the optomechanical coupling strength. We remind the reader that the true value of g is yet unknown. The CFI has its minimum for $g = 0$, meaning that the accuracy is lower when the system experiences weaker optomechanical interactions. Conversely, the CFI increases monotonically with the value of g and it reaches its maximum when the system is on the threshold of the instability.

Figure 5 shows the QFI as a function of the temperature of the mechanical bath. For high temperature, the state tends to the maximally mixed state, regardless of the value of g , and the QFI decreases. For this reason, making measurements at low temperatures increases the estimation accuracy. QFI shows a sudden drop for a temperature around 1 K. This value depends on the particular choice of the spectral density (10) of the Brownian noise and on the other parameters of the system. As expected, increasing the value of γ leads to lower values of QFI, and the accuracy of the estimation becomes worse.

V. CONCLUSIONS

In this paper, we have investigated the estimation of the optomechanical coupling strength from the perspective of classical and quantum Fisher information. We have considered a cavity quantum electrodynamical setup with a single mode of the electromagnetic field coupled to a single vibrational mode of a mechanical oscillator. Our model considers the quantum Brownian motion of the mirror and photon losses of the cavity field. We make use of the input-output formalism, motivated by the fact that experimental detection can be performed

only on the output field of the cavity. The cavity is driven by a laser, which allows us to derive a set of linear quantum Langevin equations. Under these circumstances, we have been able to obtain the output field as a Gaussian state with zero mean as a stationary solution to the evolution of the whole system.

This Gaussian state as a function of the unknown optomechanical coupling strength determines the quantum Fisher information. Here, in contrast to the typical phase-space description (see Ref. [36]), our analysis makes an explicit use of the Weyl transform. To compare with experimentally relevant scenarios, we have considered a balanced homodyne photodetection strategy as a realistic implementation for the estimation procedure. We have derived compact formulas for the quantum as well as the classical Fisher information.

Finally, we have used the developed tools to investigate situations where the classical Fisher information is capable of saturating its upper limit, given by the quantum Fisher information. To make our findings more relevant, we have taken the experimental values of the system parameters from a recent study [32]. Our results show that the phase of the local oscillator in the balanced homodyne photodetection plays a crucial role because there are certain quadratures for which the classical Fisher information can reach the value of the quantum Fisher information. Under such conditions, the accuracy of the estimation, characterized by the mean-squared error, for certain quadrature measurements has the smallest lower bound. Moreover, our investigation allows us to pinpoint the roles of the loss mechanism including less than ideal efficiency of the photodetectors. We have shown that the classical Fisher information is affected most strongly by nonideal detection efficiency. However, it is worth noticing that current state-of-the-art photodetectors have a close-to-ideal quantum efficiency [37].

In conclusion, our analysis suggests that balanced homodyne photodetection plays a fundamentally important role in the estimation of the optomechanical coupling strength. However, it must be mentioned that our work is valid only for unbiased estimators. Furthermore, finding the smallest lower bound for the mean-squared error might reinforce our prior expectation of the value of the optomechanical coupling strength, as discussed in our earlier work [9]. It is also important to mention that the use of N independent and identical repetitions of the measurement scenario reduces the lower bound of the mean-squared error by a factor of N^{-1} [4]. Finally, our work bridges cavity optomechanics and inference techniques with the help of experimentally plausible models and parameter values and could serve as a guide for the optimal experimental characterization of optomechanical systems, which play important roles in gravitational waves detection [38], but also in proposals for testing the conceptual bases of quantum mechanics [39–42].

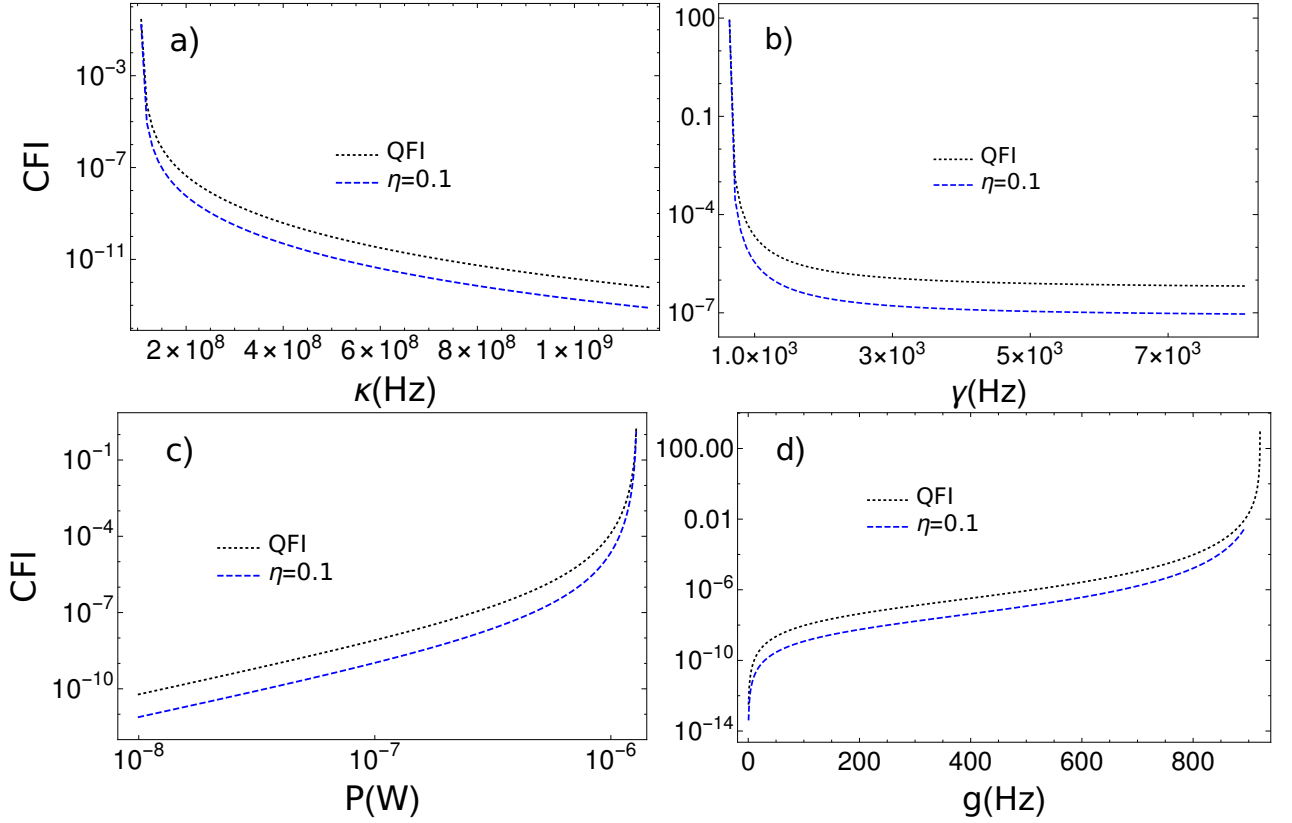


FIG. 4: Classical Fisher information (CFI) as the function of the parameters κ , γ , P and g . We set $\Delta_0 = -2\kappa$ and $\Omega_k = 0$. In the different figures we keep constant the parameter values of Fig. 1 and vary: a) the optical decay rate κ ; b) the mechanical decay rate γ ; c) the power of the driving laser P ; and in d) the value of the coupling constant g .

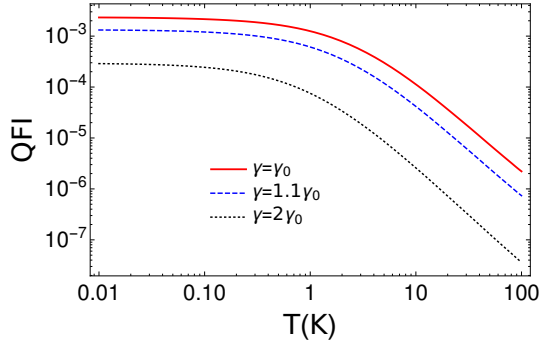


FIG. 5: Semilogarithmic plot of the quantum Fisher Information (QFI) as a function of the mechanical bath temperature T for different values of the mechanical decay rate γ . Increasing γ leads to lower values of QFI. $\gamma_0/2\pi = 130$ Hz and the rest of the parameters are the same of Fig. 1.

VI. ACKNOWLEDGEMENT

This work is supported by the European Union's Horizon 2020 research and innovation programme under Grant Agreement No. 732894 (FET Proactive HOT).

Appendix A: Dependence of the stationary field upon the laser power

The condition imposed by Eq. (14) yields a third degree equation in the mean-field amplitude $|\alpha|$. The parameter ε takes account of the number of photons inside the cavity and is related to the power P of the laser as $\varepsilon = \sqrt{\frac{2\kappa P}{\hbar\omega_L}}$. Equation (14) can be written as a function of P as

$$P = \frac{|\alpha|^6 g^4 \hbar^3 \omega_L}{2\kappa m^2 \omega_m^4} + \frac{|\alpha|^4 \Delta_0 g^2 \hbar^2 \omega_L}{\kappa m \omega_m^2} + \left(\frac{\kappa \omega_L \hbar}{8} + \frac{\Delta_0^2 \hbar \omega_L}{2\kappa} \right) |\alpha|^2 \quad (\text{A1})$$

As is typical for non-linear systems, these equations exhibit bistability. This can be seen by putting together Eqs. (A1) and (17), expressing the shift of the mirror as a function of the laser power P , resulting in

$$q_0^{(i)} = \frac{\hbar g}{m \omega_m^2} A_i, \quad i = 1, 2, 3,$$

with $A_i = |\alpha|_i^2$ being the solution of (A1). The three curves intersect when $P = P_{\pm}$,

$$P_{\pm} = \frac{m \omega_L \omega_m^2 (-2\Delta_0(4\Delta_0 + 9\kappa^2) \pm \sqrt{(4\Delta_0^2 - 3\kappa^2)^3})}{216g^2\kappa}$$

In the regions $P < P_-$ and $P > P_+$, the system is stable, but for values in between, the system admits multiple solutions for q_0 . In this work, we considered a stable solution with a power $P < P_-$ and expressed the mean value as a function of the Hamiltonian parameters, $\alpha = \alpha(g, P, \Delta_0, \kappa)$.

Appendix B: Covariance matrix of the output field

In this appendix, we derive the explicit form of the covariance matrix $\sigma_{k,\text{out}}$ of the filtered output field's quadrature $\hat{X}_{k,\text{out}}, \hat{Y}_{k,\text{out}}$. We start from the filter function,

$$g_k(t) = \frac{\theta(t+\tau) - \theta(t)}{\sqrt{\tau}} e^{i\Omega_k t},$$

where $\theta(t)$ is the Heaviside step function and τ is the temporal window when we detect the field. We consider

the detector filter function to be peaked at frequency Ω_k , with the condition that $\Omega_j - \Omega_l = \frac{2\pi}{\tau}n, n \in \mathbb{N}$. The filter function is applied to the output field \hat{a}_{out} in order to discretize the uncountably infinite number of modes forming the electromagnetic field outside the cavity into countably many modes. However, here we focus on a single mode detected by the measurement apparatus. This mode of the output field reads

$$\hat{a}_{k,\text{out}}(t) = \int_{-\infty}^t g_k(t-t') \hat{a}_{\text{out}}(t') dt'.$$

Using the input-output relation $\hat{a}_{\text{out}} = \sqrt{\kappa} \hat{a} - \hat{a}_{\text{in}}$ we can write

$$\hat{a}_{k,\text{out}}(t) = \sqrt{\kappa} \int_{-\infty}^t dt' g_k(t-t') \hat{a}(t') - \int_{-\infty}^t dt' g_k(t-t') \hat{a}_{\text{in}}(t').$$

Hence, the quadratures $\hat{X}_{k,\text{out}}, \hat{Y}_{k,\text{out}}$ read

$$\hat{X}_{k,\text{out}}(t) = \int_{-\infty}^t ds \frac{\theta(t-s) - \theta(t-s-\tau)}{\sqrt{\tau}} \left\{ \cos[\Omega_k(t-s)] \hat{X}_{\text{out}}(s) + \sin[\Omega_k(t-s)] \hat{Y}_{\text{out}}(s) \right\}$$

and, similarly,

$$\hat{Y}_{k,\text{out}}(t) = \int_{-\infty}^t ds \frac{\theta(t-s) - \theta(t-s-\tau)}{\sqrt{\tau}} \left\{ \cos[\Omega_k(t-s)] \hat{Y}_{\text{out}}(s) - \sin[\Omega_k(t-s)] \hat{X}_{\text{out}}(s) \right\}.$$

We can write the covariance matrix as

$$\begin{aligned} \sigma_{k,\text{out}}(t, s) &= \kappa \int_{-\infty}^t \int_{-\infty}^s dt' ds' \frac{\theta(t'+\tau) - \theta(t')}{\sqrt{\tau}} G_k(t-t') \langle \hat{u}(t') \hat{u}(s')^T \rangle \frac{\theta(s'+\tau) - \theta(s')}{\sqrt{\tau}} G_k(s-s')^T \\ &\quad + \int_{-\infty}^t \int_{-\infty}^s dt' ds' \frac{\theta(t'+\tau) - \theta(t')}{\sqrt{\tau}} G_k(t-t') \langle \hat{u}_{\text{in}}(t') \hat{u}_{\text{in}}(s')^T \rangle \frac{\theta(s'+\tau) - \theta(s')}{\sqrt{\tau}} G_k(s-s')^T, \end{aligned} \quad (\text{B1})$$

where $\hat{u}(t)$ and $\hat{u}_{\text{in}}(t)$ have been defined in the main text and we have introduced the matrix

$$G(t) = \begin{pmatrix} \cos \Omega_k t & \sin \Omega_k t \\ -\sin \Omega_k t & \cos \Omega_k t \end{pmatrix}.$$

Since we want to calculate the equal-time covariance matrix of the steady state, we can set $t = s$, take the limit $t \rightarrow \infty$, and substitute the Heaviside functions, yielding

$$\begin{aligned} \sigma_{k,\text{out}} &= \frac{\kappa}{\tau} \int_0^\tau \int_0^\tau dt' ds' G_k(t') \langle \hat{u}(t') \hat{u}(s')^T \rangle G_k(s')^T \\ &\quad + \frac{1}{\tau} \int_0^\tau \int_0^\tau dt' ds' G_k(t') \langle \hat{u}_{\text{in}}(t') \hat{u}_{\text{in}}(s')^T \rangle G_k(s')^T \end{aligned}$$

We suppose the detector is switched on when the system has already reached the steady state. Furthermore, we

consider the detection period τ to be small compared to the characteristic time of the steady state. This latter assumption has been tested with numerical simulations considering an integration time of the order of $\tau = \frac{1}{\kappa}$. In this scenario, we get

$$\begin{aligned} \sigma_{k,\text{out}} &= \frac{\kappa}{\tau} \int_0^\tau \int_0^\tau dt' ds' G_k(t') \sigma G_k(s')^T \\ &\quad + \frac{1}{\tau} \int_0^\tau dt' G_k(t') G_k(t')^T. \end{aligned} \quad (\text{B2})$$

After performing the integrals in Eq. (B2), we obtain the expressions (25) to (27) of the main text.

-
- [1] J. Kaipio and E. Somersalo, *Statistical and Computational Inverse Problems*, Applied Mathematical Sciences Vol. 1 (Springer-Verlag, New York, 2005).
- [2] S. D. Personick, IEEE Trans. Inf. Theory **17** (1971).
- [3] A. Holevo, J. Multivar. Anal. **3**, 337 (1973).
- [4] C. W. Helstrom, *Quantum Detection and Estimation Theory* (Academic Press, New York, 1976).
- [5] K. Macieszczak, M. Fraas, and R. Demkowicz-Dobrzański, New J. Phys. **16**, 113002 (2014).
- [6] W. Rządowski and R. Demkowicz-Dobrzański, Phys. Rev. A **96**, 032319 (2017).
- [7] J. Z. Bernád, C. Sanavio, and A. Xuereb, Phys. Rev. A **97**, 063821 (2018).
- [8] J. Rubio and J. Dunningham, New J. Phys. **21**, 043037 (2019).
- [9] J. Z. Bernád, C. Sanavio, and A. Xuereb, Phys. Rev. A **99**, 062106 (2019).
- [10] M. Aspelmeyer, T. J. Kippenberg, and F. Marquardt, Rev. Mod. Phys. **86**, 1391 (2014).
- [11] G. A. Brawley, M. R. Vanner, P. E. Larsen, S. Schmid, A. Boisen, and W. P. Bowen, Nat. Commun. **7**, 10988 (2016).
- [12] A. Bhattacharyya, Sankhā, Indian J. Stat. **8**, 1 (1946); **8**, 201 (1947).
- [13] E. W. Barankin, Ann. Math. Statist. **20**, 477 (1949).
- [14] C. R. Rao, Bull. Calcutta Math. Soc. **37**, 81 (1945).
- [15] H. Cramér, *Mathematical Methods of Statistics* (Princeton University Press, Princeton, New Jersey, 1946).
- [16] C. W. Helstrom, IEEE Trans. Inf. Theory **14**, 234 (1968).
- [17] M. G. A. Paris, Int. J. Quantum Inf. **7**, 125 (2009).
- [18] G. Casella and R. L. Berger, *Statistical inference* (Duxbury, Pacific Grove, 2002).
- [19] C. K. Law, Phys. Rev. A **49**, 433 (1994); **51**, 2537 (1995).
- [20] A. O. Caldeira and A. J. Leggett, Physica **121A**, 587 (1983).
- [21] H.-P. Breuer and F. Petruccione, *The theory of open quantum systems* (Oxford University Press, Oxford, 2002).
- [22] D. F. Walls and G. J. Milburn, *Quantum Optics* (Springer-Verlag, Berlin, 1994).
- [23] A. I. Lvovsky and M. G. Raymer, Rev. Mod. Phys. **81**, 299 (2009).
- [24] A. K. Tagantsev and S. A. Fedorov, Phys. Rev. Lett. **123**, 043602 (2019).
- [25] H.-P. Breuer, B. Kappler and F. Petruccione, Ann. Phys. **291**, 36 (2001).
- [26] V. Giovannetti and D. Vitali, Phys. Rev. A **63**, 023812 (2001).
- [27] A. Garg, J. N. Onuchic, and V. Ambegaokar, J. Chem. Phys. **83**, 4491 (1985).
- [28] M. Abramowitz and I. A. Stegun, *Handbook of Mathematical Functions* (Dover Publ., New-York, 1968).
- [29] F. R. Gantmacher, *Applications of the Theory of Matrices* (Wiley, New York, 1959).
- [30] C. Genes, A. Mari, P. Tombesi, and D. Vitali, Phys. Rev. A **78**, 032316 (2008).
- [31] G. Adam, J. Mod. Opt. **42**, 1311 (1995).
- [32] M. Rossi, D. Mason, J. Chen, and A. Schliesser, Phys. Rev. Lett. **123**, 163601 (2019).
- [33] M. Karuza, C. Biancofiore, M. Galassi, R. Natali, G. Di Giuseppe, P. Tombesi and D. Vitali, AIP Conference Proceedings **1**, 1363 (2011).
- [34] R. A Horn and C. R. Johnson, *Matrix Analysis* (Cambridge University Press, Cambridge UK, 1999).
- [35] L.-H. Zhang, Comput. Optim. Appl. **54**, 111 (2013).
- [36] A. Monras, arXiv:1303.3682 (2013).
- [37] S. Daiss, and S. Welte, and B. Hacker, and L. Li, and G. Rempe, Phys. Rev. Lett. **122**, 133603 (2019).
- [38] B. P. Abbott et al. (LIGO Scientific Collaboration and Virgo Collaboration), Phys. Rev. Lett. **116**, 061102 (2016).
- [39] W. Marshall, C. Simon, R. Penrose, D. Bouwmeester, Phys. Rev. Lett. **91**, 130401 (2003).
- [40] S. L. Adler, A. Bassi, and E. Ippoliti, J. Phys. A **38**, 2715 (2005).
- [41] J. Z. Bernád, L. Diósi, T. Gészti, Phys. Rev. Lett. **97**, 250404 (2006).
- [42] S. McMillen, M. Brunelli, M. Carlesso, A. Bassi, H. Ulbricht, M. G. A. Paris, and M. Paternostro, Phys. Rev. A **95**, 012132 (2017).